Peer-reviewed version available at *Molecules* **2018**, *23*, 1781; doi:10.3390/molecules23071781

DFT simulations of the vibrational spectrum and hydrogen bonds of ice XIV

Kai Zhang, Peng Zhang*, Ze-Ren Wang, Xu-Liang Zhu, Ying-Bo Lu, Cheng-Bo Guan, Yanhui Li

School of Space Science and Physics, Shandong University, Weihai, 264209, China

Abstract

It is always a difficult task to assign the peaks recorded from vibrational spectrum. Herein we explored a new pathway of density functional theory (DFT) simulation to present three kinds of spectra of ice XIV and can be referenced as inelastic neutron scattering (INS), IR, and Raman experimental spectrum. The INS spectrum is proportional to phonon density of states (PDOS) while the photon scattering signals reflect the normal vibration frequencies near the Brillouin zone (BZ) center. Based on good agreements with experimental data, we identified the relative frequency and made scientific assignments by normal vibration modes analysis. The debating two hydrogen bond (H-bond) peaks among ice phases from INS have been discussed and the dynamic process of H-bond vibrations were found to be classified into two basic modes. we deduce that two H-bond modes are a general rule among ice family and more works are ongoing to investigate this subject.

Keywords: ice XIV, vibrational spectrum, hydrogen bond, CASTEP, first-principles, DFT

1. Introduction

Water is not only an essential resource for the survival of all life, but also the most important part of living organisms. The solid state of water, ice, has been discovered more than 19 different crystal phases and amorphous structures under certain pressure and temperature [1-10]. Usually they are paired of hydrogen-ordered and hydrogen-disordered and can transform each other at specific ambient condition. To facilitate the study of normal vibration modes of ice, a hydrogen-ordered structure is beneficial to calculation and presents the main physical features due to its simple primitive cell [12].

In 1998, Lobban and co-workers first reported the identification of a new ice phase named ice XII that crystallized at 260 K and 0.55 GPa [7]. In 2006, Salzmann et al. found that ice XII doped with HCl would transform into a new hydrogen-ordered phase upon cooling under pressure, which was called ice XIV with space group $P2_12_12_1$ symmetry [8,13]. Later, Raman spectrum and inelastic neutron scattering of ice XIV/XII have been reported [14-19].

In spite of many references presented experimental vibrational spectra of ice XIV/XII, theoretically method to assign the peaks is lack of report till now. Herein we calculated the most stable XIV structure by using first-principles density functional theory (DFT) to manifest the vibrational spectrum assisted by normal vibrational modes analysis.

2. Computational Methodology

Based on DFT method of quantum mechanics, the CASTEP [20] code is used to perform geometric optimization and phonons calculation on structure of ice XIV. According to our test, the XC function of GGA RPBE [21] is selected for geometry

Peer-reviewed version available at Molecules 2018, 23, 1781; doi:10.3390/molecules23071781

optimization. The energy and SCF tolerance should take the minimum values for phonons calculation. The energy cutoff is 750 eV, and the K-point grid is $2 \times 2 \times 3$ in the reduced BZ. The norm-conserving pseudo potentials are used to calculate the PDOS and polarizability. The environmental pressure is set as 0.55 GPa.

3. Results and Discussion

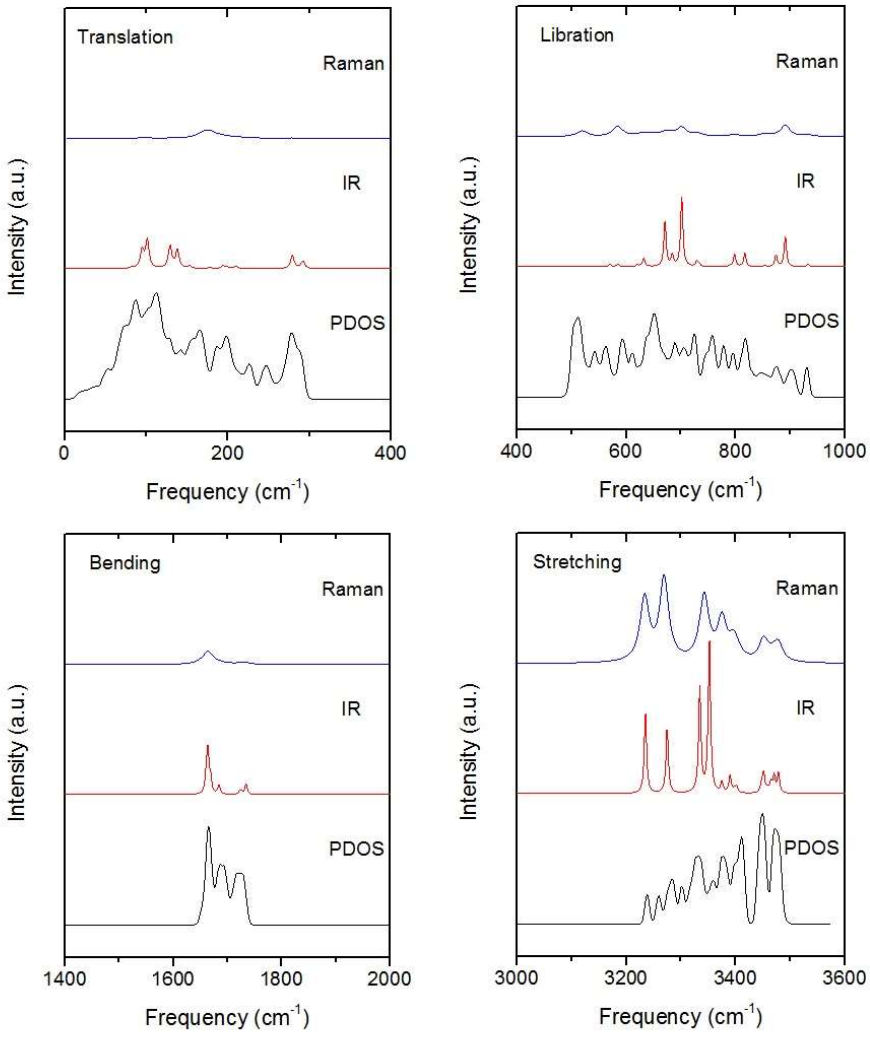

Figure1. The simulated spectrum of ice XIV. Four images correspond to four vibration bands: translation, libration, bending and stretching. Each image from top to bottom is Raman, IR, and PDOS spectrum. Weak peaks have been amplified reasonably.

The computational spectra of Raman, IR and PDOS are ranked in Fig.1 by four separate bands. Because the spectrum intensities of Raman and IR have a quite large scale, the relative proportions of two spectra in each band have been adjusted for comparisons. The PDOS spectrum as well as normal vibration frequencies are calculated after precise geometry optimization. In theory, the spectrum by INS is proportional to PDOS, whilst the photon scattering can only collect signals near BZ center. Table 1 presents comparisons of the PDOS against neutron scattering, and the normal vibration frequencies against Raman scattering. Since ice XIV is hydrogen-ordered phase of ice XII, the spectrum of XIV shows pronounced features than XII. Both of the Raman spectra of ice XIV and XII then could be used for peaks assignement. There are 12 molecules in a primitive cell of ice XIV. Thus the number of optic normal modes is 12×3×3-3=105. Each band of the spectrum is discussed in detail as follows.

Table 1. Comparison of calculated results with Raman and INS data. The main peak of PDOS in the first column is compared against INS spectrum. The frequencies of 105 normal vibration modes are compared with the Raman data. The unit of data is cm^{-1}.

PDOS	**Neutr. Scattering (ref.17/18)**	**Normal modes**	**Raman scattering (ref.13/14/16)**
53	56/—	62	
75	80/—	82	
		83	
		84	
88	96/—	90	
		92	
		94	
		95	
104		100	
		101	
		102	

113		104	
128		127	
		128	
		129	
142		138	
		153	
159	160/—	154	
166		162	
		169	
		176	
		178	214/195/192
188	192/—	192	
		193	
		194	
199	—/~208	199	
		209	
226		211	241/—/—
248		236	
		277	314/—/—
279		279	
288	—/~288	289	
		292	
504	~464/—	502	
512		510	
		518	462/470/490
		523	
		524	488/—/—
543		545	
563	~560/—	570	
		583	527/—/—
		585	562/553/—
593		591	
612		613	
		620	
		625	
		631	
		632	
639	~632/—	642	
		643	
652		657	

		671	
688		684	
		695	
		701	
705		702	
725		724	
		729	
748		733	
757	~760/—	751	
777		790	
796		798	790/—/—
817		817	
846		845	
		853	
876		874	
903	~904/—	891	867/—/—
930		932	
		933	
		1647	
		1661	
1665		1663	
		1668	
		1669	
		1671	
1687		1684	
1693		1705	
1720		1722	
1727		1725	
		1734	
		1735	
		3234	3214/3209/3215
3238		3235	
3260		3269	3317/3310/—
3283		3275	
3302		3322	
3333		3334	
		3343	3326/—/—
		3351	
3358		3352	
		3375	3346/3340/—

3376	3377	~3348/—/—
	3390	
	3395	3368/—/—
3400	3398	
	3402	
3411	3411	
	3447	
3449	3450	
	3451	~3407/3415/3410
	3458	
	3465	
	3467	
3473	3470	
	3478	

The stretching band is the region of O-H covalent bond stretching. There are 24 normal vibration modes and the frequencies of mode range from 3234 cm^{-1} to 3478 cm^{-1}. Each molecule has two kinds of vibration: symmetric stretching and asymmetric stretching. As shown in Fig. 2, there are two molecular vibration images corresponding to the minimum and maximum vibration frequencies, respectively. This is a top view and the green arrows represent the vibration direction in sizes proportional to the vibration amplitude. For the minimum mode at 3234 cm^{-1}, there are four molecules present symmetric stretching vibration, two examples are illustrated in gold. It has been found for ice XV that some modes include the isolated vibration of only one O-H bond while the other one does not vibrate [22]. This is a similar case in ice XIV. We attribute this exotic phenomenon to geometry deformation of local tetrahedron structure under pressure. Almost all molecules are asymmetric stretching at 3478 cm^{-1}, which consistent with literature that the energy increasing from symmetric stretching to

Peer-reviewed version available at *Molecules* **2018**, *23*, 1781; doi:10.3390/molecules23071781

asymmetric stretching. To maintain a static center of mass, the vibrations of molecule are correlated in a primitive cell. An obvious phenomenon is that Raman and IR spectrum are more sensitive to symmetric stretching. From the spectrum of Fig.1, one can see several distinct peaks in the symmetric stretching region due to the restrictions of selection rules.

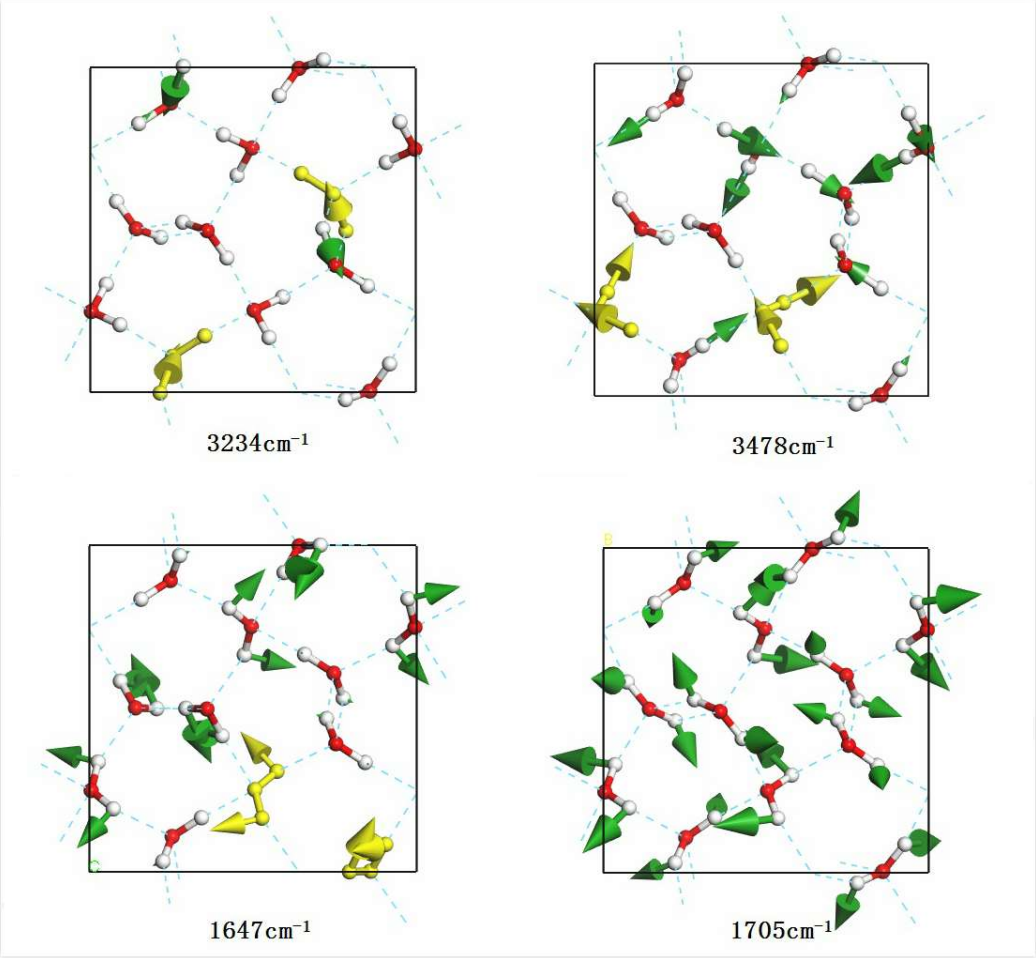

Figure 2. A top view of four normal vibration modes in stretching band (3234 cm^{-1}, 3478 cm^{-1}) and bending band (1647 cm^{-1}, 1705 cm^{-1}), respectively. Typical vibrations are represented in gold. The green arrows represent the vibration direction in sizes proportional to the vibration amplitude.

Salzmann et al. recorded the Raman spectrum of recovered hydrogen ordered ice XIV and identified the vibration modes by deuterated method [14]. By comparison, they detected six Raman peaks at 3214 cm^{-1}、3317 cm^{-1}、3326 cm^{-1}、3346 cm^{-1}、3368 cm^{-}

[1] and ~3407 cm^{-1} are good agreement with this work at 3234 cm^{-1}、3269 cm^{-1}、3343 cm^{-1}、3375 cm^{-1}、3395 cm^{-1}、3451 cm^{-1} (Table 1). They reported that the peak at 2480 cm^{-1} of D_2O was not observed at 2480×1.35=3348 cm^{-1} in H_2O of ice XIV. According to Fig. 1, we found that the peak should be at 3377 cm^{-1} (normal mode). Salzmann et al. also performed Raman spectrum of ice XII [14], of which peaks at 3209 cm^{-1}、3310 cm^{-1}、3340 cm^{-1}、3415 cm^{-1} are consistent with normal mode at 3234 cm^{-1}, 3269 cm^{-1}, 3375 cm^{-1}, 3451 cm^{-1}, respectively.

In the intramolecular bending vibration band, there are 12 normal vibration modes ranging from 1647 cm^{-1} to 1735 cm^{-1}. Considering a collective vibration, all the bending modes can be classified as in-phase and out-of-phase vibrations. Fig.2 shows two bending vibration images at frequencies of 1647 cm^{-1} and 1705 cm^{-1}. The molecules in gold at 1647 cm^{-1} shows a pair of out-of-phase modes. According to our previous work, we found that the energy increasing trend is from in-phase bending to out-of-phase bending. However, for the case of ice XIV, the lowest mode at 1647 cm^{-1} shows four pairs of out-of-phase vibrations. The vibration mode at 1705 cm^{-1} shows in-phase vibrating of all molecules. Although the simulated Raman and IR spectrum both contain a peak at 1663 cm^{-1}, the intensity is too weak to be detected IR.

As for the intermolecular librational band, there are 36 normal modes and the frequencies range from 502 cm^{-1} to 933 cm^{-1}. In this region, all the molecular vibration modes could be classified into three types: rocking, twisting, and wagging. A rocking mode is oscillating in plane whilst a wagging is oscillating perpendicular to the molecular plane. A twisting mode is a rotation around the bisector of angle. For the

mode at 656 cm^{-1} in Fig. 3, the highlighted molecule shows wagging vibration while the 695 cm^{-1} mode presents combinations of rocking and twisting. Interestingly, we found that all molecules are rocking at 523 cm^{-1} and all molecules are wagging at 933 cm^{-1}, which means that the energy of rocking is lower than wagging. From simulated Raman spectrum we only see four weak peaks and the IR spectrum has three sharp peaks at 671 cm^{-1}, 701 cm^{-1}, and 890 cm^{-1}, which are the combinations of three vibration types.

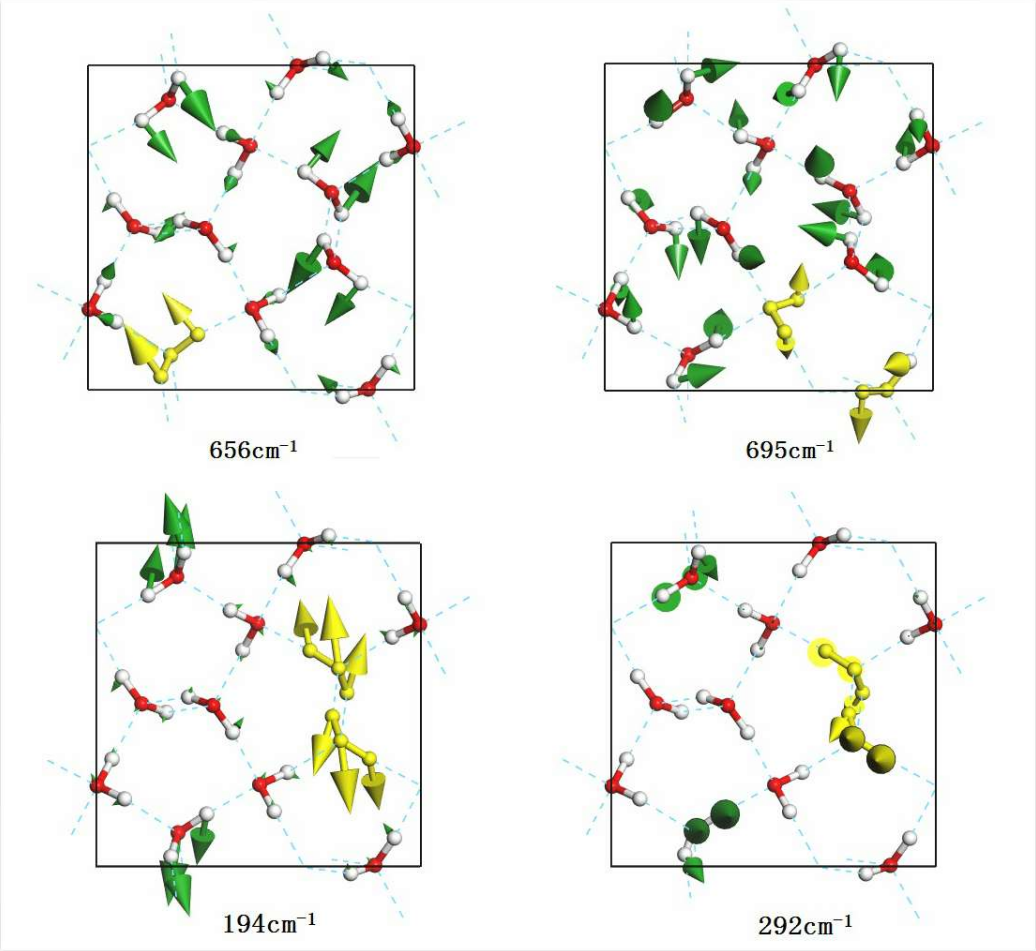

Figure 3. A top view of four normal vibration modes in libration band (656 cm^{-1}, 695 cm^{-1}) and translation band (194 cm^{-1}, 291 cm^{-1}), respectively. For the dynamic process of weak and strong H-bond, please see the supplemental movies of 194.avi and 292.avi.

Compared with experimental data, six vibration peaks (462 cm^{-1}, 488 cm^{-1}, 527 cm^{-}

^{1}, 562 cm^{-1}, 790 cm^{-1}, 867 cm^{-1}) from Raman scattering [14] are agreement with normal mode calculations（518 cm^{-1}、524 cm^{-1}、583 cm^{-1}、585 cm^{-1}、798 cm^{-1}、891 cm^{-1}）. However, a peak recorded at 413 cm^{-1} could not be assigned from simulations. We suspect this was a false peak according to DFT simulations. The peak at 470 cm^{-1} (Ref. 15)/490 cm^{-1} (Ref. 17) should be frequency at 518 cm^{-1} (normal mode in Table 1). As for the INS spectrum, we can roughly match the peaks of ~464 cm^{-1}, ~560 cm^{-1}, ~632 cm^{-1}, ~760 cm^{-1}, ~904 cm^{-1} (Ref. 18) to 504 cm^{-1}、563 cm^{-1}、639 cm^{-1}、757 cm^{-1}、903 cm^{-1} (PDOS).

In the intermolecular translational band, there are 33 normal vibration modes range from 62 cm^{-1} to 292 cm^{-1}. For one molecule, there exist three vibration modes: stretching, wagging and rocking. Note that, a rocking in the translational band is monolithic movement whilst a rocking in the librational band is only hydrogen vibration within one molecule. To date, the physical mechanism of H-bond interaction is still a question [22-25]. Li et al. proposed a two-stkerength model based on electrostatic interactions to explain the two main peaks from INS spectrum [26,27]. The model has not been widely accepted which is still a controversial topic [28-31]. He et al. disagreed this model and asserted these two peaks originated from the different directionalities of motion manifested in the distinct polarizations of absorbed photons [31]. In the previous study, we found that the two H-bond peaks in the hydrogen-ordered ice Ic are originated from two different H-bond vibration modes. There are four H-bonds linked with one molecule to form a tetrahedral structure in ice crystal. For ice Ic, there are two kinds of vibration modes for one molecule: two H-

bond vibrating mode and four H-bond vibrating mode with a strength ratio of $\sqrt{2}$ [32]. These two types of modes are also observed in ice XIV crystal lattice. In the translational band of Fig. 1, the peak of maximum strength observed at 288 cm^{-1} is very distinct. Phonons at above ~200 cm^{-1} are main four H-bond vibrations analyzed by normal vibration modes. Example of vibration mode at 292 cm^{-1} in Fig. 3 shows that molecules are stretching along its bisector of angle. This is a typical four H-bond vibration mode in which four linked H-bond are oscillating together. The two H-bond mode means that one molecule vibrates toward connected neighbour in which there are two effective H-bonds oscillating for this mode. Subject to local tetrahedral structure, the collective vibrations are combinations of wagging and rocking as illustrated in Fig. 3 of mode at 194 cm^{-1}. To show dynamic process of these two modes, please see the videos from supplemental files. For ice XIV, the local structure can not maintain a regular tetrahedron due to lattice deformation under pressure. Thus, deviations strength ratio from $\sqrt{2}$ are reasonable. From Fig. 1, it can be seen that there are two main peaks at 166 cm^{-1} and 199 cm^{-1}. Phonons around this region are mainly two H-bond modes. There are other vibration modes associated with clusters vibration or skeleton deformation below 166 cm^{-1}. These optic phonons are merged with acoustic phonons.

In the simulated Raman spectrum of Fig.1, there is a small peak at 176 cm^{-1}. It should be corresponding to experimental observations at 192/195/214 cm^{-1} [17, 15, 14]. The red-shift is mainly due to the RPBE function has a bit underestimate for H-bond [13]. As for INS spectrum, two distinct peaks at 26 meV and 36 meV (204 cm^{-1} and 288 cm^{-}

^{1}) [18] are agreement with 204 cm^{-1} and 288 cm^{-1} (PDOS). Koza et al. mentioned several peaks in the far-IR region, such as 7 meV, 10 meV, 12 meV, 24 meV (56 cm^{-1}, 80 cm^{-1}, 96 cm^{-1}, 192 cm^{-1}) [18]. They could be matched with 53 cm^{-1}, 75 cm^{-1}, 88 cm^{-1}, 188 cm^{-1} (PDOS in Table 1).

4. Conclusions

In summary, by using the first-principles DFT method, we present Raman scattering, IR absorption, and INS spectrum (PDOS) of ice XIV theoretically. The PDOS spectrum is used to assign the characteristic peaks in INS spectrum because the INS collect signals throughout the whole BZ without selection so that the simulated PDOS spectrum is proportional to INS. The 105 optic normal vibration modes in the BZ center could be compared with Raman and IR spectra. Under this condition, the peaks recorded from photon scattering could be assigned according to normal vibration mode individually.

The most valuable result is the identification of two types of H-bond vibration modes. The thermodynamic nature of H-bond is a fascinating but still ambiguous topic to date. Inspired by previous study on ice Ic, we concluded that there are also two types of H-bond vibration modes in ice XIV. Deviations are mainly result from structure deformation of local regular tetrahedron under pressure. Considering the local structure symmetry, we deduce that the two H-bond modes is a general rule among ice family and more works are ongoing to investigate this subject.

Peer-reviewed version available at *Molecules* **2018**, *23*, 1781; doi:10.3390/molecules23071781

Supplementary Materials: The following are available online at www.mdpi.com/xxx/s1, Video S1: Dynamic process of H-bond vibration at 292 cm^{-1}. Video S2: Dynamic process of H-bond vibration at 194 cm^{-1}.

Authors' contributions. K.Z performed simulations and drafted the manuscript. P.Z conducted simulations, data analysis and edited the manuscript. Z-R. W and X-L. Z assisted structure modeling and data processing. Y-B. L, C-B. G and Y-H. L participated results discussion. All the authors gave final approval for publication.

Founding: This research was funded by National Natural Science Foundation of China grant number 11504202.

Acknowledgments. The numerical calculations were done on the supercomputing system in the Supercomputing Center, Shandong University, Weihai.

References

1. Bertie, J.E.; Whalley, E. Optical Spectra of Orientationally Disordered Crystals. II. Infrared Spectrum of Ice Ih and Ice Ic from 360 to 50 cm^{-1}, *J. Chem. Phys.* **1967**, 46, 1271-1284.
2. Bertie, J.E.; Calvert, L.D.; Whalley, E. Transformations of Ice II, Ice III, and Ice V at Atmospheric Pressure, *J. Chem. Phys.* **1963**, 38, 840-846.
3. Kuhs, W.F.; Finney, J.L.; Vettier, C.; Bliss, D.V. Structure and hydrogen ordering in ices VI, VII, and VIII by neutron powder diffraction, *J. Chem. Phys.* **1984**, 81, 3612-3623.
4. Whalley, E.; Heath, J.B.R.; Davidson, D.W. Ice IX: An Antiferroelectric Phase Related to Ice III, *J. Chem. Phys.* **1968**, 48, 2362-2370.

5. Tajima, Y.; Matsuo, T.; Suga, H. Phase transition in KOH-doped hexagonal ice, *Nature* **1982**, 299, 810-812.
6. Hirsch, K.R.; Holzapfel, W.B. Effect of high pressure on the Raman spectra of ice VIII and evidence for ice X, *J. Chem. Phys.* **1986**, 84, 2771-2775.
7. Lobban, C.; Finney, J.L.; Kuhs, W.F. The structure of a new phase of ice, *Nature* **1998**, 391, 268-270.
8. Salzmann, C.G.; Radaelli, P.G.; Mayer, A.E.; Finney, J.L. The Preparation and Structures of Hydrogen Ordered Phases of Ice, *Science* **2006**, 311, 1758-1761.
9. Salzmann, C.G.; Radaelli, P.G.; Mayer, E.; Finney, J.L. Ice XV: a new thermodynamically stable phase of ice, *Phys. Rev. Lett.* **2009,** 103, 105701-105704.
10. Falenty, A.; Hansen, T.C.; Kuhs, W.F. Formation and properties of ice XVI obtained by emptying a type sII clathrate hydrate, *Nature* **2014**, 516, 213-233.
11. del Rosso, L.; Celli, M.; Ulivi, L. New porous water ice metastable at atmospheric pressure obtained by emptying a hydrogen-filled ice, *Nat. Comm.* **2016**, 7, 13394-13400.
12. Zhang, P.; Wang, Z.; Lu, Y.B.; Ding, Z.W. The normal modes of lattice vibrations of ice XI, *Sci. Rep.* **2016**, 6, 29273-29281.
13. Tribello, G.A.; Slater, B.; Salzmann, C.G. A Blind Structure Prediction of Ice XIV, *J. AM. Chem. Soc.* **2006**, 128, 12594-12595.
14. Salzmann, C.G.; Hallbrucker, A.; Finney, J.L.; Mayer, E. Raman spectroscopic features of hydrogen-ordering in ice XII, *Chemical Physics Letters.* **2006**, 429, 469-473.

15. Salzmann, C.G.; Kohl, I.; Loerting, T.; Mayer, E.; Hallbrucker, A. The Raman Spectrum of Ice XII and Its Relation to that of a New "High-Pressure Phase of H_2O Ice", *J. Phys. Chem. B.* **2002**, 106, 1-6.

16. Yoshimura, Y.; Stewart, S.T.; Mao, H.-K.; Hemley, R.J. In situ Raman spectroscopy of low-temperature/high-pressure transformations of H_2O, *J. Chem. Phys.* **2007**, 126, 174505-174512.

17. Chou, I.-M.; Blank, J.G.; Goncharov, A.F.; Mao, H.-K.; Hemley, R.J. In Situ Observations of a High-Pressure Phase of H_2O Ice, *Science* **1998**, 281, 809-812.

18. Koza, M.M.; Schober, H.; Tölle, A.; Fujara, F.; Hansen, T.; Formation of ice XII at different conditions, *Nature* **1999**, 397, 660-661.

19. Koza, M.M.; Schober, H.; Parker, S.F.; Peters, J. Vibrational dynamics and phonon dispersion of polycrystalline ice XII and of high-density amorphous ice, *Phys. Rew. B.* **2008**, 77, 104306-104314.

20. Clark, S.J.; Segall, M.D.; Pickard, C.J.; Hasnip, P.J.; Probert, M.I.J.; Refson, K.; Payne, M.C. First principles methods using CASTEP, *Z. Kristallogr.* **2005**, 220, 567-570.

21. Hammer, B.; Hansen, L.B.; Norskov, J.K. Improved adsorption energetics within density-functional theory using revised Perdew-Burke-Ernzerhof functionals, Phys. Rev. B. 59 (1999) 7413-7421.

22. Whale, T.F.; Clark, S.J.; Finney, J.L.; Salzmann, C.G.; DFT-assisted interpretation of the Raman spectra of hydrogen-ordered ice XV, *J. Raman. Spectroscopy.* **2013**, 44, 290-298.

23. Klug, D.D.; Whalley, E. Origin of the High-Frequency Translational Bands of Ice I. *J. Glaciol.* **1978**, 21, 55-63.

24. Marchi, M.; Tse, J.S.; Klein, M.L.; Lattice vibrations and infrared absorption of ice Ih, *J. Chem. Phys.* **1986**, 85, 2414-2418.

25. Tse, J.S.; Klug, D.D. Comments on "Further evidence for the existence of two kinds of H-bonds in ice Ih" by Li et al, *Phys. Lett. A.* **1995**, 198, 464-466.

26. Li, J.C.; Ross, D.K. Evidence for two kinds of hydrogen bond in ice, *Nature* **1993**, 365, 327-329.

27. Li, J.C. Inelastic neutron scattering studies of hydrogen bonding in ices, *J. Chem. Phys.* **1996**, 105, 6733-6755.

28. Klotz, S.; Strassle, T.; Salzmann, C.G.; Philippe, J.; Parker, S.F. Incoherent inelastic neutron scattering measurements on ice VII: Are there two kinds of hydrogen bonds in ice? *Europhys. Lett.* **2005**, 72, 576-582.

29. Zhang, P.; Tian, L.; Zhang, Z.P.; Shao, G.; Li, J.C. Investigation of the hydrogen bonding in ice Ih by first-principles density function methods, *J. Chem. Phys.* **2012**, 137, 044504-044508.

30. Zhang, P.; Han, S.H.; Yu, H.; Liu, Y. A calculating proof on hydrogen bonding in ordinary ice by the first-principles density functional theory, *RSC Adv.* **2013**, 3, 6646-6649.

31. He, X.; Sode, O.; Xantheas, S.S.; Hirata, S. Second-order many-body perturbation study of ice Ih, *J. Chem. Phys.* **2012**, 11, 204505-204512.

32. Yuan, Z.Y.; Zhang, P.; Yao, S.K.; Lu, Y.B.; Yang, H.Z.; Luo, H.W.; Zhao, Z.J.

Computational assignments of lattice vibrations of ice Ic, *RSC Adv.* **2017**, 7, 36801-36806.